Publications of the Astronomical Society of the Pacific
105: 117–122, 1993 January

Main-Beam Efficiency Measurements of the Caltech Submillimeter Observatory

JEFFREY G. MANGUM[1]

Department of Astronomy, The University of Texas, Austin, Texas 78712
Electronic mail: jmangum@heineken.tuc.nrao.edu

Received 1992 August 14; accepted 1992 October 9

ABSTRACT. We report main-beam efficiency measurements at 211–365 GHz of the Caltech Submillimeter Observatory (CSO). These calculations are based on antenna temperature measurements of Mars, Jupiter, Saturn, and the Moon. We also present an analysis and review of the broadband millimeter and submillimeter continuum emission properties of Mars, Jupiter, Saturn, and the Moon. Through this analysis we establish a set of recommended main-beam efficiencies for the facility receivers at the CSO.

1. INTRODUCTION

Source antenna temperature measurements done at millimeter and submillimeter wavelengths are telescope dependent. To facilitate comparison between measurements done using different telescopes, one must measure the beam efficiency. The beam efficiency is dependent upon a number of parameters, including the angular extent of the source being measured. Therefore, the most accurate estimate of the beam efficiency of a telescope at millimeter and submillimeter wavelengths is made by measuring a number of sources with differing known source sizes. This can best be accomplished by measuring the continuum emission from the Moon and planets. In this paper, we report measurements of the main-beam efficiency over a range of frequencies and source sizes for the Caltech Submillimeter Observatory. We also present some useful information regarding the use of Mars, Jupiter, Saturn, and the Moon as calibration sources.

2. OBSERVATIONS

The Caltech Submillimeter Observatory (CSO) is a 10.4-m radio telescope located near the summit of Mauna Kea, Hawaii. A description of the technical specifications of the CSO can be found in Serabyn et al. (1991). The measurements that we present in this paper were made using the facility 230 and 345 GHz receivers over the period 1989 January–1992 February. The backends employed were 50 and/or 500 MHz acousto-optical spectrometers (AOS). Calculations of the main-beam efficiency are based on position-switched measurements of the antenna temperatures of Mars, Jupiter, Saturn, and the Moon. For the planetary measurements, the OFF position was located 5′ in azimuth away from the ON position. For the Moon measurements the OFF position was situated 1° in azimuth away from the ON position.

[1]Current address: University of Arizona, Steward Observatory, Submillimeter Telescope Observatory, Tucson, AZ 85721.

3. THE TECHNIQUE

Raw data at the CSO is written using the telescope-dependent T_A^* temperature scale. In order to compare measurements made using different telescopes, one must measure the "beam efficiency" in order to translate ones data to the telescope-independent T_R scale [see Kutner and Ulich (1981) for a detailed discussion of temperature scales]. The two scales are related by

$$T_R=\frac{T_A^*}{\eta_c\eta_{\rm fss}}$$

where η_c is the source-coupling efficiency and $\eta_{\rm fss}$ is the forward spillover and scattering efficiency. In general, η_c will depend on the coupling of the telescope beam to the source. For this reason it is convenient to factor η_c into two terms: a source-filling factor (f_s) and a term which describes the coupling to a source which just fills the main beam, which we will call η_c (main beam):

$$\eta_c=f_s\eta_c(\text{main beam}).$$

This allows us to define the main-beam efficiency $\eta_{\rm mb}$:

$$\eta_{\rm mb}=\eta_c(\text{main beam})\eta_{\rm fss},$$

which leads to the definition of the main-beam brightness temperature

$$T_{\rm mb}=\frac{T_A^*}{\eta_{\rm mb}}.$$

One can tie this definition to the original definition of the beam efficiency (η_b) by noting that η_b includes the rear scattering and spillover efficiency ($\eta_{\rm rss}$). Therefore, $\eta_{\rm mb}$ is actually $\eta_b/\eta_{\rm rss}$. Referring to the recent discussion of radio-astronomical temperature scales by Gordon et al. (1992), our definition of $\eta_{\rm mb}$ corresponds to the term η_B' used in their analysis.

By measuring T_A^* on a planet or the Moon, one can derive $\eta_{\rm mb}$ using the following:

© 1993. Astronomical Society of the Pacific

© Astronomical Society of the Pacific • Provided by the NASA Astrophysics Data System

$$\eta_{mb}=\frac{\frac{1}{2}T_A^*(\text{source})}{J(\nu_s,T_{source})-J(\nu_s,T_{cmbr})}\times\left[1-\exp\left(-\ln 2\,\frac{\theta_{eq}\theta_{pol}}{\theta_{mb}^2}\right)\right]^{-1}, \quad (1)$$

which is the convolution of a Gaussian telescope beam with a uniform disk source. The terms in this equation are defined as follows:

$J(\nu,T_B)\equiv$Planck function at frequency ν and brightness temperature $T_B=\dfrac{h\nu/k}{\exp(h\nu/kT_B)-1}$;

$T_A^*(\text{source})\equiv$single-sideband antenna temperature of calibration source;

$T_{source}\equiv$brightness temperature of calibration source;

$T_{cmbr}\equiv$brightness temperature of the cosmic microwave background ($\sim$2.78 K);

$\theta_{eq}\equiv$equatorial diameter of calibration source;

$\theta_{pol}\equiv$poloidal diameter of calibration source;

$\theta_{mb}\equiv$telescope main-beam FWHM.

T_{source} can be found in the literature or calculated directly (see Secs. 4 and 5), θ_{eq} and θ_{pol} can be found in the Astronomical Almanac, and θ_{mb} can be derived from the following relation assuming a diffraction-limited beam with a uniform illumination pattern and 10 dB taper on the edges:

$$\theta_{mb}=1.17\left(\frac{\lambda}{D}\right)\text{ radians}=\frac{72348.267}{\nu D}\text{ arcsec},$$

where ν is in GHz and D in meters.

The term involving T_{cmbr} takes into account the fact that when you position switch on an opaque object like a planet, you are actually measuring the difference between T_A^* (source) and the temperature of the cosmic-microwave background radiation. The cosmic-microwave background term contributes $<1\%$ to the $J(\nu_s,T_{source})-J(\nu_s,T_{cmbr})$ term, so it can generally be ignored. Using the Rayleigh–Jeans approximation to $J(\nu_s,T_{source})$ results in an $\sim$2%–6% overestimation of this term for measurements of Mars, Jupiter, and Saturn in the 200–365 GHz range.

To first order, η_{mb} as calculated above is the beam efficiency ($\eta_c\eta_{fss}$) appropriate for objects with sizes equal to θ_{mb}. To second order, η_{mb} as calculated above is the beam efficiency appropriate for objects approximately equal in size to the calibration source. For example, η_{mb} calculated using Jupiter is not really an appropriate beam efficiency for objects $\gg\theta_{Jupiter}$ or objects $\ll\theta_{Jupiter}$. Under these circumstances, one of the following calculations must be done:

(1) For objects $\ll\theta_{Jupiter}$ one should use η_{mb} measured on a smaller planet, like Mars, and correct the temperature measurements by the filling factor for your source and beam:

$$\eta_{small\ source}=\eta_{mb}(\text{Mars})\left(\frac{\theta_s}{\theta_{mb}}\right)^2.$$

(2) For objects $\gg\theta_{Jupiter}$ one should use η_{mb} measured on a larger planet. Unfortunately, there are no planets larger than Jupiter, so one must use η_{mb} derived from Moon measurements:

$$\eta_{large\ source}=\eta_{mb}(\text{Moon}).$$

Note that because the moon is so large (30′), use of a moon-derived η_{mb} will *underestimate* T_R because of the inclusion of the beam sidelobes in the T_A^* measurement. Note also that if you use the moon as your calibration source, you will actually be measuring just η_{fss}, since η_c (main beam) = 1 for sources much larger than the beam. Information regarding the use of the moon as a calibration source is given in Sec. 5.

TABLE 1
Jovian Planet Brightness Temperatures

Planet	Mean frequency (GHz)	Bandwidth (GHz)	T_{planet} (K)	Reference[a]
Jupiter				
	31	···	152.4± 4.8	1
	86	···	180.4± 4.7	3
	90	···	172.5± 1.4	3
	90	···	179.4± 4.7	1
	150	···	167.0±12.0	1
	150	50	173.3± 1.1	3
	227	70	170.9± 3.9	3
	279	75	169.9± 5.1	3
	310	130	175.0±10.0	2
	337	150	174.3± 5.1	3
	392	75	162.5± 2.0	3
	451	270	167.1± 2.1	2
	580	420	149.9± 2.6	2
	666	170	135.0± 5.0	2
	674	90	148.5± 4.9	3
	724	625	155.3± 1.3	2
	808	200	143.7± 1.9	3
	849	250	165.5± 2.5	2
	865	110	145.1± 2.3	3
	870	57	139.5± 3.8	3
Saturn				
	31	···	133.0± 4.2	1
	90	···	149.3± 4.1	1
	150	···	137.0±11.0	1
	310	130	134.5± 3.2	2
	451	270	137.0± 4.0	2
	580	420	122.2± 1.1	2
	666	170	112.3± 3.2	2
	724	625	119.2± 1.2	2
	849	250	112.9± 1.1	2

[a]References: 1. Ulich (1981); 2. Hildebrand et al. (1985); 3. Griffin et al. (1986).

4. CALIBRATION SOURCE TEMPERATURES

In the following we discuss a few things that one should be aware of regarding the use of Mars, Jupiter, and Saturn as calibration sources. In Table 1 we list brightness temperatures for Jupiter and Saturn.

4.1 Mars Brightness Temperatures

Because Mars is bright, compact, and has a solid surface and only a tenuous atmosphere, it is generally used as the flux calibration standard at far infrared through millimeter

© Astronomical Society of the Pacific • Provided by the NASA Astrophysics Data System

wavelengths. Using results from the Mariners 6 and 7 spacecraft, Neugebauer et al. (1971) (see also Wright 1976; Wright and Odenwald 1980; Simpson et al. 1981) developed a model of the Martian far-infrared thermal emission. This model does not include the influences of a dusty atmosphere or of the Martian polar caps. At wavelengths shorter than 40 μm, atmospheric dust storms may have a direct influence on the Martian thermal-continuum emission. These effects should be negligible at longer wavelengths because of the λ^{-1} dependence of the continuum optical depth unless, as pointed out by Griffin et al. (1986), the thermal emission at longer wavelengths is diminished due to reduced solar insolation during a dust storm. With these provisos in mind, a reasonably accurate calibration scale can be constructed based on the model-predicted continuum brightness of Mars. In our calculation of η_{mb} using measurements of the Martian brightness temperature, we have used the Neugebauer et al. model to derive T_{Mars}.

It is instructive to point out that Ulich (1981) showed that the Martian brightness temperature at 3.3 mm is given by

$$T(R)=T(R_0)\sqrt{\frac{R_0}{R}},$$

where $R_0=1.524$ AU (mean Martian heliocentric distance), $T(R_0)=206.8\pm5.8$ K, and $T(R)=$Martian brightness temperature at heliocentric distance R. Brightness temperatures predicted by the Neugebauer et al. model are usually within 10% of those predicted by the expression above. $T(R_0)$ agrees well with the Neugebauer et al. model for the far-infrared emission, indicating that the global temperature changes very slowly with increasing wavelength and that the Martian thermal emission closely approximates a blackbody at millimeter and submillimeter wavelengths.

4.2 Molecular Absorption Lines in the Spectra of Jupiter and Saturn

Most of the measurements of the brightness temperatures of Jupiter and Saturn are broadband continuum measurements. The bandwidths in these measurements are generally some 100's of GHz; i.e., one brightness temperature for the entire 345 GHz window. Since models of the atmospheric continuum emission at millimeter wavelengths indicate that the brightness temperature changes very little over a given band, broadband measurements of T_{source} are sufficient for calculations of η_{mb}. One physical effect that the broadband measurements cannot measure, though, is the existence of molecular-absorption features superimposed on the continuum emission spectrum of the planet. At selected frequencies, these features can decrease the planetary brightness temperature by as much as 15% for Jupiter and 40% for Saturn [see Lellouch et al. (1984) for details]. The most dominant absorption lines are from HCN, PH_3, and NH_3. In the 230 and 345 GHz windows, one might expect to see strong absorption at 266 GHz (HCN $J_L=2$ and PH_3 $J_L=0$) and 354 GHz (HCN $J_L=3$). The HCN $J_L=2$ and PH_3 $J_L=0$ transitions subtract $\gtrsim 10\%$ of the brightness temperature of Jupiter for $264\lesssim\nu\lesssim268$ GHz and of Saturn for $257\lesssim\nu\lesssim275$ GHz. The HCN $J_L=3$ transition subtracts $\gtrsim 10\%$ of the brightness temperatures for Jupiter and Saturn in the frequency range $350\lesssim\nu\lesssim355$ GHz. Note that both of the estimates for Jupiter neglect the possible importance of H_2S on the jovian infrared spectrum (see Lellouch, et al. Combes 1984).

4.3 Saturn's Rings

Ulich (1981), Hildebrand et al. (1985), and Epstein (1980) have analyzed the affects of Saturn's rings on the measured brightness temperature of Saturn. When the rings are at low inclination ($\sim2^\circ\lesssim$ inclination $\lesssim20^\circ$) they block a small fraction of the Saturnian disk (since the rings are colder than the planet surface). For larger inclinations, the rings begin to add emission to the disk because they begin to be projected off the planetary disk. In general, based on the Epstein et al. models, these effects represent $\lesssim 10\%$ corrections to the millimeter continuum brightness temperature of Saturn for ring inclinations $\lesssim 30^\circ$. Unfortunately, the 3 mm continuum measurements of Ulich (1981) do not agree with the model predictions of Epstein et al. and are instead consistent with no ring emission. Our own measurements of the main-beam efficiency using Saturn during a period when the ring inclination was about 20° are generally *lower* than efficiency measurements made using measurements of Jupiter or Mars (see Sec. 6). Our current recommendation is to avoid the use of Saturn as a calibrator until these effects are understood.

5. USING THE MOON AS A CALIBRATION SOURCE

Efficiencies based on lunar emission measurements require an analysis of the lunar emission properties. A complete discussion and analysis of these properties has been given by Krotikov and Troitskiĭ (1964) and Linsky (1966, 1973). In the following, we present a review of this work.

The properties of the thermal radio emission from the Moon are determined by the conditions under which the surface layer becomes heated and cooled during the course of a lunation. The behavior of this emission as a function of lunar phase is determined by the electric and thermal properties of the lunar surface material. Following Krotikov and Troitskiĭ (1964) and Linsky (1966, 1973), we assume that the lunar surface is smooth and uniform with temperature- and depth-independent thermal properties. The surface temperature as a function of depth, longitude, latitude, and time $T(x,\phi,\psi,t)$ can be found by solving the equation of heat conduction

$$\rho c(x,t)\frac{\partial T(x,\phi,\psi,t)}{\partial t}=\frac{\partial}{\partial x}\left(\kappa(x,t)\frac{\partial T(x,\phi,\psi,t)}{\partial x}\right),$$

where ρ, $c(x,t)$, and $\kappa(x,t)$ are the density, specific heat, and conductivity of the lunar surface material. The most convenient form for the solution to this equation is a Fourier series

© Astronomical Society of the Pacific • Provided by the NASA Astrophysics Data System

TABLE 2
Values for $T_0(0)$[a]

λ	12 μm	17.5 μm	30 μm	100 μm	300 μm	1 mm	3 mm
$T_0(0)$	213.9±6.0	212.7±6.2	213.7±8.7	216.1±6.9	217.6±8.1	219.1±6.3	227.7±8.9

[a]From Linsky (1973), Table 6.

$$T(x,\phi,\psi,t)=T_0(\psi)+\sum_{n=1}^{\infty}(-1)^{a_n}T_n(\psi)\times\exp\left[-x\left(\frac{nP}{2\alpha}\right)^{1/2}\right]\times\cos\left[n\Phi-n\phi-\phi_n-x\left(\frac{nP}{2\alpha}\right)^{1/2}\right].$$

Therefore, the thermal radio-brightness temperature at position (ϕ,ψ) is given by

$$\begin{aligned}T_R(\lambda,\phi,\psi,t)&=[1-R(\phi,\psi)]\int_0^{\infty}T(x,\phi,\psi,t)k_\lambda\sec(r)\times\exp[-xk_\lambda\sec(r)]dx\\&=[1-R(\phi,\psi)]\Bigg(T_0(\psi)+\sum_{n=1}^{\infty}\frac{(-1)^{a_n}T_n(\psi)}{[1+2\delta_n(\lambda)\cos(r)+2\delta_n^2(\lambda)\cos^2(r)]^{1/2}}\times\cos[n\Phi-n\phi-\phi_n-\xi_n(\lambda,\phi,\psi)]\Bigg),\end{aligned}$$

where

$R(\phi,\psi)\equiv$reflection coefficient of the lunar surface;
$k_\lambda\equiv$coefficient of electromagnetic wave absorption;
$r\equiv$angle between the normal to the surface and the direction at the point of reception;
$T_0(\psi)\equiv$average (over one lunar period) brightness temperature;
$a_n\equiv\dfrac{(n-1)(n-2)}{2}$;
$\delta_n(\lambda)\equiv\sqrt{\dfrac{nP}{2\alpha}}=$ratio of the thermal attenuation coefficient for the nth Fourier component to the electromagnetic attenuation coefficient;
$\Phi\equiv 2\pi t/P$;
$\phi_n\equiv$phase shift relative to insolation for the nth Fourier component of the surface temperature;

$$\xi_n(\lambda,\phi,\psi)\equiv\tan^{-1}\left(\frac{\delta_n(\lambda)\cos(r)}{1+\delta_n(\lambda)\cos(r)}\right)=\text{phase}$$

shift relative to insolation for the nth Fourier component of the radio brightness temperature.

At the center of the lunar disk $(\phi,\psi)=(0,0)$ and for a given time t, this equation reduces to the following:

$$T_R(\lambda)=(1-R_0)\Bigg(T_0(0)+\sum_{n=1}^{\infty}\frac{(-1)^{a_n}T_n(0)}{[1+2\delta_n(\lambda)+2\delta_n^2(\lambda)]^{1/2}}\times\cos[n\Phi-\phi_n-\xi_n(\lambda,0,0)]\Bigg).$$

The harmonic amplitudes for $n>1$ are only a small fraction of the $n=1$ harmonic amplitude and can be ignored. Also, $R_0\leqslant 0.05$ (Linsky 1973), so that $1-R_0\simeq 1$. These two assumptions reduce our equation for $T_R(\lambda)$ to the following:

$$T_R(\lambda)=T_0(0)+\frac{T_1(0)}{[1+2\delta_1(\lambda)+2\delta_1^2(\lambda)]^{1/2}}\times\cos[\Phi-\phi_1-\xi_1(\lambda,0,0)].$$

Measurements of the radio emission from the Moon extrapolated to $\lambda=0$ have been used to derive values for $T_1(0)$ in terms of $T_0(0)$ and $\delta_1(\lambda)$. Linsky (1966) finds that $T_1(0)/T_0(0)=0.77$ and $\delta_1(\lambda)\simeq 0.24\lambda$ (λ in mm). Therefore, our equation for $T_R(\lambda)$ becomes

$$T_R(\lambda)=T_0(0)+\frac{0.77T_0(0)}{(1+0.48\lambda+0.11\lambda^2)^{1/2}}\times\cos[\chi-\xi_1(\lambda,0,0)],\qquad(2)$$

where

$$\chi\equiv\Phi-\phi_1=\left(\frac{\text{days since new Moon}}{\text{period of Moon}}\right)\times 360-180,$$

$$\xi_1(\lambda,0,0)\equiv\tan^{-1}\left(\frac{0.24\lambda}{1+0.24\lambda}\right),$$

period of Moon=29.530589 days.

This equation should be applicable throughout the radio and infrared wavebands. Values for $T_0(0)$ (from Linsky 1973, Table 6) are given in Table 2.

6. THE MEASUREMENTS

Table 3 lists measurements of η_{mb} made over the period 1989 January–1992 February. Each entry has been calculated using the following technique. For each measurement of a calibration source, T_A^* and an rms uncertainty have been estimated. When a scan was taken using both the 50 and 500 MHz AOS, the average between these two measurements was used. η_{mb} was then calculated for each measurement along with an uncertainty based on the noise using either Eq. (1) for planet measurements or Eq. (2)

© Astronomical Society of the Pacific • Provided by the NASA Astrophysics Data System

TABLE 3
CSO Main-Beam Efficiency

Source	Date	$\theta_{eq}\times\theta_{pol}$[a] (arcsec^2)	θ_{mb} (arcsec)	T_A^*(source) (K)	T_{source} (K)	ν (GHz)	η_{mb}
Mars							
	01/91	12.3×12.2	21.0	36.5± 1.5	196.3± 9.8[b]	330.5	0.46±0.02
	07/90	8.3×8.2	20.1	31.5± 1.5	227.6±11.4[b]	345.7	0.66±0.03
	07/90	8.3×8.2	20.1	33.5± 1.0	227.6±11.4[b]	345.8	0.69±0.02
	01/89	8.3×8.2	20.1	24.0± 1.5	228.0±11.0[b,c]	345.9	0.50±0.03
	01/91	12.8×12.8	20.1	38.5± 1.0	196.3± 9.8[b]	345.9	0.42±0.02
	07/90	8.3×8.3	19.7	33.5± 0.5	227.6±11.4[b]	353.0	0.66±0.04
	07/90	8.3×8.3	19.5	33.0± 0.5	227.6±11.4[b]	356.7	0.64±0.02
Jupiter							
	11/91	34.1×31.8	31.9	126.0± 1.0	169.9± 5.1	218.2	0.73±0.02
	02/92	44.2×41.3	31.9	157.0± 3.0	169.9± 5.1	218.2	0.67±0.02
	11/91	33.7×31.6	31.8	125.0± 1.0	169.9± 5.1	218.4	0.74±0.01
	02/92	44.2×41.3	31.7	172.0± 5.0	170.9± 3.9	219.6	0.72±0.03
	02/92	44.2×41.3	31.6	170.0± 5.0	170.9± 3.9	220.4	0.71±0.03
	02/92	44.2×41.3	31.6	185.5± 2.0	169.9± 5.1	244.9	0.71±0.02
	06/92	36.4×34.0	25.0	168.0± 2.0	169.9± 5.1	278.7	0.69±0.02
	02/92	43.9×41.1	21.0	182.5± 7.5	175.7± 5.1	330.6	0.58±0.02
	01/91	45.5×42.5	20.9	147.0± 5.0	173.9± 5.1	332.3	0.46±0.01
	03/90	39.8×37.3	20.8	153.0± 8.0	174.1± 5.1	335.0	0.51±0.03
	03/90	39.3×36.8	20.4	140.5± 3.5	173.4± 5.1	341.3	0.47±0.01
	02/92	43.8×41.0	20.2	171.0± 3.0	173.0± 5.1	342.9	0.54±0.01
	02/92	44.2×41.3	20.1	173.0± 7.5	172.4± 5.2	345.8	0.55±0.02
	01/89	43.8×41.0	20.1	163.5± 3.0	172.4± 5.2	345.9	0.52±0.01
	01/90	46.6×43.6	20.0	165.0± 7.0	171.9± 5.2	348.3	0.52±0.02
	01/90	46.6×43.6	19.9	170.5± 1.0	171.7± 5.2	349.3	0.54±0.01
	02/90	43.3×40.5	19.6	176.0± 2.0	170.5± 5.4	354.6	0.57±0.01
	03/90	39.3×36.8	19.6	131.5± 2.5	170.5± 5.4	354.8	0.44±0.01
	01/91	45.3×42.3	19.6	186.5± 2.0	170.5± 5.4	355.0	0.59±0.01
	03/90	39.8×37.3	19.5	142.5± 2.5	170.2± 5.4	356.0	0.47±0.01
	11/91	34.1×31.8	19.2	159.0± 5.0	168.8± 5.7	362.7	0.57±0.02
	02/92	44.1×41.2	19.2	171.5± 2.5	168.8± 5.7	362.7	0.55±0.02
	02/90	42.5×39.7	19.1	185.0± 7.0	168.5± 5.8	364.1	0.60±0.03
	02/92	44.0×41.1	19.1	166.5± 5.5	168.5± 5.8	364.1	0.54±0.03
	02/90	42.5×39.7	19.0	164.0± 9.5	168.2± 5.8	365.4	0.53±0.03
Saturn							
	08/91	18.3×16.5	33.0	24.5± 0.5	134.5± 3.2	211.2	0.54±0.02[d]
	10/91	17.2×15.6	33.0	24.5± 1.0	134.5± 3.2	211.2	0.60±0.03
	08/91	18.2×16.5	32.3	25.0± 2.0	134.5± 3.2	215.4	0.53±0.04[d]
	08/91	18.3×16.5	31.9	27.0± 2.0	134.5± 3.2	218.2	0.56±0.04[d]
	08/91	18.3×16.5	31.8	22.0± 2.0	134.5± 3.2	218.4	0.46±0.04[d]
	08/91	18.3×16.5	31.7	25.0± 1.0	134.5± 3.2	219.6	0.51±0.02[d]
	10/91	17.1×15.5	31.7	31.0± 1.0	134.5± 3.2	219.6	0.72±0.03
	08/91	18.2×16.5	31.6	27.0± 1.0	134.5± 3.2	220.4	0.55±0.02[d]
	10/91	17.1×15.5	31.6	29.5± 0.5	134.5± 3.2	220.4	0.68±0.02
	07/91	18.5×16.7	30.8	26.0± 2.0	134.5± 3.2	225.7	0.50±0.04[d]
	08/91	18.3×16.5	30.8	27.0± 2.0	134.5± 3.2	225.7	0.53±0.03[d]
	08/91	18.3×16.5	28.4	26.5± 2.0	134.5± 3.2	244.9	0.45±0.03[d]
	07/91	18.5×16.7	20.3	46.5± 4.0	134.5± 3.2	342.9	0.45±0.04
	10/91	17.2×15.6	20.3	34.5± 3.5	134.5± 3.2	342.9	0.38±0.05
Moon							
	08/91	13.9 days	28.4	545.0± 5.0	335.9± 9.7	244.9	0.83±0.03
	03/90	17.6 days	20.8	512.0±11.0	343.5± 9.9	335.0	0.76±0.02
	03/90	15.0 days[e]	20.5	545.0±14.0	355.1±10.2	338.5	0.78±0.02
	07/90	15.0 days[e]	20.1	544.0± 5.5	355.7±10.2	345.7	0.78±0.01
	01/90	15.0 days[e]	20.0	534.0± 5.0	355.9±10.2	348.3	0.77±0.01
	01/90	15.0 days[e]	19.9	489.5± 6.0	356.0±10.2	349.3	0.70±0.01
	03/90	15.0 days[e]	19.5	540.0± 5.0	356.6±10.2	356.0	0.78±0.02

[a]For moon measurements, we list the number of days since new moon.
[b]Uncertainty assumed to be ±5%.
[c]Extrapolated from 1990 model predictions.
[d]Old 230 GHz receiver (before 10/91).
[e]Measurement made at the subsolar point, so age given as 15.0 days (full moon).

© Astronomical Society of the Pacific • Provided by the NASA Astrophysics Data System

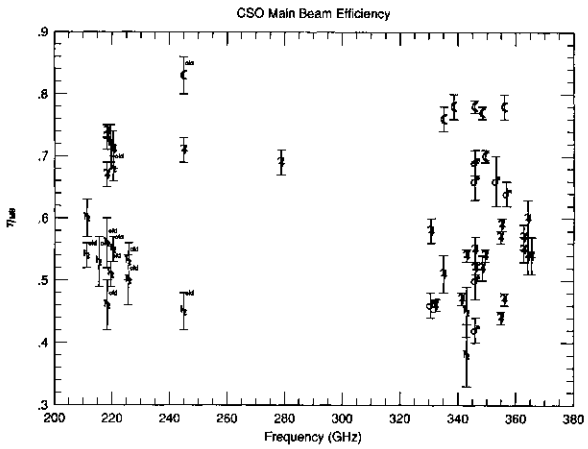

FIG. 1—Main-beam efficiency measurements for the facility 230 and 345 GHz receivers at the Caltech Submillimeter Observatory. Individual measurements are plotted using the appropriate astronomical symbol for the measured source. Measurements denoted as "old" were obtained using the old facility 230 GHz receiver, which was operational until 1991 October.

for Moon measurements. Then, for a given observing run and frequency, a statistical average η_{mb}, an rms uncertainty calculated from the uncertainties in the individual measurements, and a standard deviation calculated from the variance of the individual measurements was calculated. These average values are given in Table 3, where the uncertainty for each entry is the greater of the rms uncertainty and the standard deviation of the individual measurements. In general, the standard deviation is more than twice the rms uncertainty, suggesting that systematic effects like pointing, sideband gain, atmospheric stability, etc., are the main sources of uncertainty. In the calculation of η_{mb} from Jupiter measurements, we have used a linearly interpolated value for T_{source} from the measurements of Griffin et al. (1986) (see Table 1). Martian brightness temperatures are taken from calculations based on the Neugebauer et al. (1971) model of the martian thermal emission. A plot of the average η_{mb} values given in Table 3 as a function of frequency is shown in Fig. 1.

7. RECOMMENDATIONS

Our measured values for η_{mb} using a given calibration source are reasonably constant within the tuning range for a particular receiver. Therefore, we list in Table 4 average values for η_{mb} applicable to each receiver along with the standard deviation due to dispersion from run to run and over frequency for a given receiver. In the absence of direct measurements, the efficiencies in Table 4 should be used. The efficiency measurements made using Saturn are generally lower than those from measurements of Jupiter and Mars. This may be due to the effects of Saturn's rings on measurements of the thermal continuum emission (see Sec. 4.3). Because of these uncertainties, we recommend that observers avoid the use of Saturn as a calibrator.

TABLE 4
Average CSO Main-Beam Efficiencies

Source	Receiver[a]	Average η_{mb}	No. of measurements[b]
Mars	345	0.57±0.11	7
Jupiter	new 230	0.71±0.02	7
	345	0.53±0.05	18
Saturn	old 230	0.51±0.05	9
	new 230	0.67±0.06	3
	345	0.41±0.05	2
Moon	new 230	0.83±0.03	1
	345	0.76±0.03	6

[a]The old 230 GHz receiver was operational until 1991 October.
[b]This is the number of measurements which went into the calculation of the average.

I would like to thank Todd Groesbeck for providing me with several of the antenna temperature measurements used in this paper. I also thank Neal Evans for useful comments regarding efficiency measurements and for suggesting that I publish this work. This work was supported in part by Texas Advanced Research Program grant 003658-285 and National Science Foundation grant AST-9017710 to the University of Texas.

REFERENCES

Epstein, E. E., Janssen, M. A., Cuzzi, J. N., Fogarty, W. G., and Mottmann, J. 1980, Icarus, 41, 103
Gordon, M. A., Baars, J. W. M., and Cocke, W. J. 1992, A&A, in press
Griffin, M. J., Ade, P. A. R., Orton, G. S., Robson, E. I., Gear, W. K., Nolt, I. G., and Radostitz, J. V. 1986, Icarus, 65, 244
Hildebrand, R. H., Loewenstein, R. F., Harper, D. A., Orton, G. S., Keene, J., and Whitcomb, S. E. 1985, Icarus, 64, 64
Krotikov, V. D., and Troitskiĭ, V. S. 1964, Soviet Phys.-Usp. (Engl. Transl.), 6, 841
Kutner, M. L., and Ulich, B. L. 1981, ApJ, 250, 341
Lellouch, E., Encrenaz, T., and Combes, M. 1984, A&A, 140, 405
Linsky, J. L. 1966, Icarus, 5, 606
Linsky, J. L. 1973, ApJS, 25, 163
Neugebauer, G., Münch, G., Kieffer, H., Chase, Jr. S. C., and Miner, E. 1971, AJ, 76, 719
Serabyn, E., Phillips, T. G., and Masson, C. R. 1991, Appl. Opt. 30, 1227
Simpson, J. P., Cuzzi, E. F., Erickson, E. F. Strecker, D. W., and Tokunaga, A. T. 1981, Icarus, 48, 230
Ulich, B. L. 1981, AJ, 86, 1619
Wright, E. L. 1976, ApJ, 210, 250
Wright, E. L., and Odenwald, S. 1980, BAAS, 12, 456

© Astronomical Society of the Pacific • Provided by the NASA Astrophysics Data System